Energy 72 (2014) 501–509

Contents lists available at ScienceDirect

Energy

journal homepage: www.elsevier.com/locate/energy

Hybrid-input power supply with PFC (power factor corrector) and MPPT (maximum power point tracking) features for battery charging and HB-LED driving

Chih-Lung Shen*, Yong-Xian Ko

Department of Electronic Engineering, National Kaohsiung First University of Science and Technology, No.1, University Rd., Yanchao Dist. Kaohsiung City 82445, Taiwan

ARTICLE INFO

Article history:
Received 16 February 2014
Received in revised form
18 April 2014
Accepted 17 May 2014
Available online 18 June 2014

Keywords:
Hybrid input
Power factor correction
PV power
Dual outputs

ABSTRACT

In this paper, a MSEBC (modified-SEPIC embedded-boost converter) is proposed, which can deal with either utility power or PV (photovoltaic) power to serve as HB-LED (High-Brightness Light-Emitting-Diode) driver and battery charger. While connected to utility, the proposed converter can perform PFC (power factor corrector) for universal line input. Once power failure occurs, it can draw energy from PV panel with MPPT (maximum power point tracking). Even if there is no utility power and PV energy, the MSEBC still can power on HB-LED from battery bank to achieve uninterruptable lighting feature. The topology of MSEBC is mainly derived from SEPIC-type converter as well as an embedded boost converter to develop a single-stage configuration, instead of multi-stage or two-stage type. Even though it only has single stage, both functions of HB-LED driving and battery charging still can be accomplished. In the MSEBC, a coupled inductor is adopted to replace the second inductor of traditional SEPIC and the chock of boost converter. A microprocessor-based controller is developed to accomplish all converter functions. A prototype, which have the functions of dealing with universal line input 85 ~ 265 V_{rms}, performing power factor correction, tracking maximum power for PV panel, lighting HB-LED, and charging/discharging battery, is carried out. Key measurements have verified the feasibility, functionality, and validity.

1. Introduction

AC-to-DC power supplies are wide used to electric vehicles, electric appliances, industry applications, and lighting system. Generally, they include a front-end diode rectifier, resulting in current harmonics and power pollution. Therefore, PFC (power factor corrector) is required to wave-shape the input current to be sinusoidal as well as to improve power factor. PFCs have two categories. One is passive PFC and the other is active PFC. Without the need of active switch and associated control circuit, passive PFC has the advantage of lower cost. However, it cannot achieve power factor as high as active one so that active PFC still is the major adoption in market products. Among active-PFC configurations, boost type attracts a great deal of interests owing to its high-power-factor ability and easy control [1–4]. The output voltage of a boost converter can be larger than input [5,6]. It pops up the necessary of a step-down stage cascaded between the PFC and a low-voltage load. That is, two-stage structure dominates low-voltage power supply.

In the literature [7,8], power processing through two stages will lower overall conversion efficiency. Some researchers pay attentions to single-stage configuration. Even though the single-stage converter derived from buck-boost topology resolves the problem that PFC steps up input voltage [9–13], reverse polarity at output port causes another issue. Flyback PFC can avoid the mentioned problem [14,15], nevertheless which exists the demerits of low efficiency and pulsating input current. SEPIC topology can be another selection [16,17], but the disadvantages of limited functions, single input, and unidirectional power follow processing will confine its applications.

Recently, the development regarding renewable energy and energy-saving lighting system attracts a lot of attentions. The system of a battery bank charged by PV arrays is presented in Refs. [18,19] but there is no the mechanism relating to battery discharge. In Refs. [20–24], the power supply systems, which can deal with PV (photovoltaic) power, battery energy, and HB-LED driving, are proposed. Nevertheless, their configurations are two-stage and incapable of drawing power from utility.

* Corresponding author. Tel.: +886 7 6011000; fax: +886 7 6011386.
E-mail address: clshen@nkfust.edu.tw (C.-L. Shen).

http://dx.doi.org/10.1016/j.energy.2014.05.072

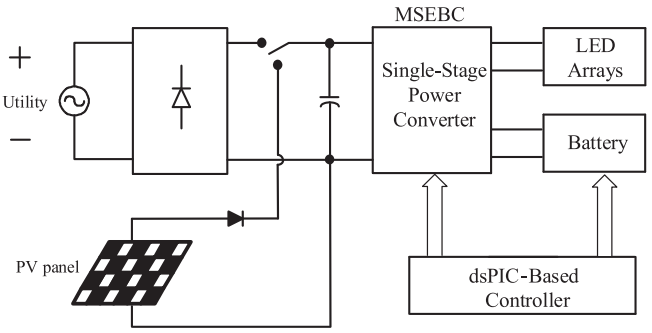

Fig. 1. A block diagram to illustrate the configuration of the proposed MSEBC.

This paper proposes a novel single-stage converter, which not only can deal with universal line input and PV power but accomplish the features of power factor correction, MPPT (maximum power point tracking), HB-LED driving, and battery charging/discharging. The proposed converter is derived from the integration of an SEPIC converter and a boost converter, so called MSEBC (modified-SEPIC embedded-boost converter). The input of MSEBC can be either universal line input or PV panel. While dealing with line input, the proposed converter corrects power factor. While drawing power from PV panel, the converter can fulfill MPPT. With respect to output, the converter has two output ports. One drives HB LEDs and the other performs battery charging simultaneously. In MSEBC, a coupled inductor is adopted to replace the second inductor of the SEPIC and the choke of the boost converter such as to reduce volume and to develop dual-output configuration. A prototype of MSEBC is designed, analyzed, simulated, and measured. Practical measurements have demonstrated the feasibility of the proposed converter.

2. Configuration of power stage

Fig. 1 shows a block diagram to represent the configuration of the proposed MSEBC. The converter is a single-stage structure, of which input terminal can be connected to either utility or PV panel. It has two output ports for powering HB-LED arrays and charging battery bank simultaneously. A dsPIC-based controller is developed to function all converter features. The corresponding circuitry of the main power stage is shown in Fig. 2. The input inductor L_1, active switch Q_1, capacitor C_1, diode D_5, and coupled inductor develop an SEPIC-type configuration, which have two output ports so as to drive HB LEDs and charge battery. The secondary of the coupled inductor, diode D_6, and active switch Q_2 form a boost-type converter to discharge battery energy for LED driving. The Q_3 serves as a relay. During the interval of battery discharging, the Q_3 is kept in on-state in order to loop a discharging path.

The MSEBC has three operation modes: utility mode, PV mode, and discharging mode. In utility mode, a conceptual diagram to represent power flow direction is illustrated in Fig. 3. In this mode, utility supplies energy to LED arrays and battery. While operating in PV mode, only PV panel is in charge of power-supply task for LED arrays and battery, as shown in Fig. 4. If encountering both situations of power failure and no irradiation, the MSEBC is capable of performing uninterruptible lighting by drawing power from battery to LEDs. Fig. 5 illustrates the corresponding power flow direction.

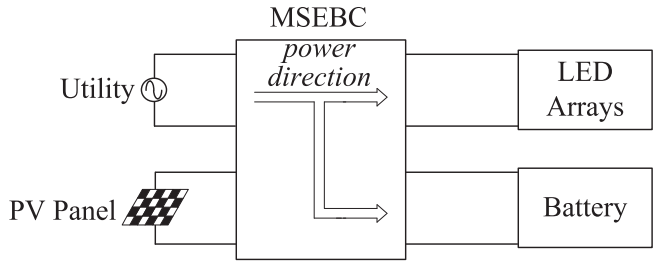

Fig. 3. A diagram to illustrate the power flow direction while the MSEBC works at utility mode.

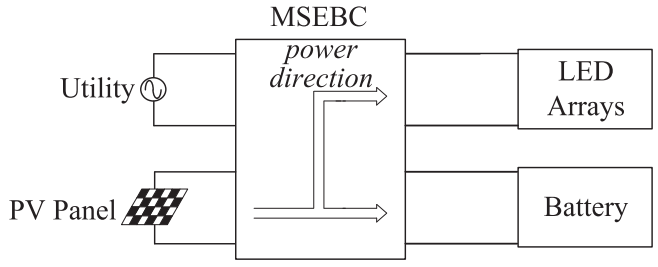

Fig. 4. A diagram to illustrate the power flow direction while the MSEBC works at PV mode.

3. Operation principle of MSEBC

As mentioned in Section 2, the MSEBC has three operation modes. According to on/off statuses of the active switches in MSEBC, we can classify these operation modes into two categories, Condition 1 and Condition 2. Utility mode and PV mode are classified to be Condition 1, while charging mode is Condition 2. Table 1 depicts this classification.

3.1. Condition 1

When operated at utility mode or PV mode, the MSEBC shown in Fig. 2 can be simplified to Fig. 6. In utility mode, the MSEBC functions as a single-stage PFC, but in PV mode, it is an MPPT dc/dc converter. Under both modes, Q_2 and Q_3 are in off-state. On the contrary, Q_1 is switched at high frequency much higher than line frequency so as to wave-shape and to control input current for

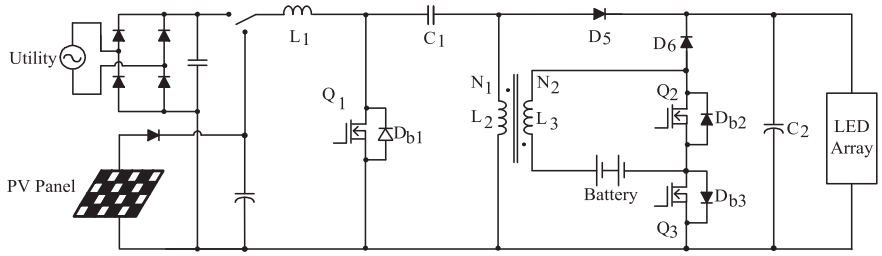

Fig. 2. The circuitry of the main power stage of MSEBC.

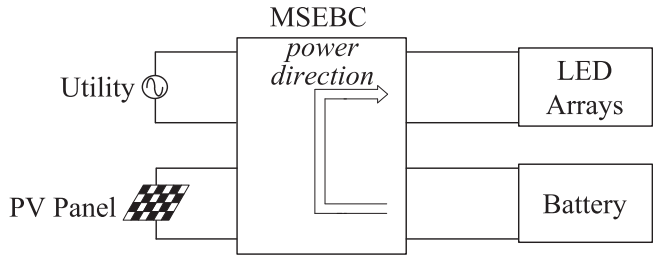

Fig. 5. A diagram to illustrate the power flow direction while the MSEBC works at discharging mode.

Table 1
The depiction of the classification based on switch on/off status.

Condition 1	Utility mode	Q_1: Switched at high frequency Q_2 and Q_3: Always off
	PV mode	Q_1: Switched at high frequency Q_2 and Q_3: Always off
Condition 2	Discharging mode	Q_1: Always off Q_2: Switched at high frequency Q_3: Always on

power factor correcting or maximum power point tracking. According to Q_1 on and off, over one switching cycle, there are two major operation stages, which are discussed as follows:

1) Stage 1 [Q_1 on, see Fig. 7(a)]:

At this stage, since the switch Q_1 is on, the input voltage directly crosses on the inductor L_1. The input voltage over a switching period can be regarded as a constant and then inductor current i_{L1} is linearly built by v_s. At the same time, the capacitor C_1 dumps energy to the inductor L_2 and the output capacitor C_2 supplies energy to LED arrays. The time constant of the output loop is determined by the capacitance of C_2 and the load resistance. Assume that this time constant is much larger than switching period. Thus, output voltage v_o will be invariant during a switching cycle.

In stage 1, applying Kirchhoff's voltage law to the input loop, the i_{L1} can be calculated by

$$i_{L1}(t) = i_{L1}(t_0) + \int_{t_0}^{t} \frac{v_S(t') - V_{DS1,on}}{L_1} dt' \quad (1)$$

where the initial value of inductor current $i_{L1}(t_0)$ is found by the end of stage 2 of Condition 1 and $V_{DS1,on}$ denotes the on-state voltage drop of the Q_1. The $i_{L1}(t_0)$ will be zero if the converter performs power factor correction under BCM (boundary-current-mode) or DCM (discontinuous-current-mode) control. In addition, the current following through L_2, i_{L2}, is built by the voltage v_{c1}, which is estimated as follows:

$$i_{L2}(t) = i_{L2}(t_0) + \int_{t_0}^{t} \frac{v_{c1}(t') - V_{DS1,on}}{L_2} dt' \quad (2)$$

Similarly, the $i_{L2}(t_0)$ is the initial current of inductor L_2, which is determined by the end of stage 2. The ripple frequency of capacitor C_1 is much less than the switching frequency. Therefore, over one switching period the voltage v_{c1} is considered to be invariant and thus i_{L2} is increased linearly. The relationship between input v_s and output v_{c2} is expressed as

$$v_{C2}(t) = v_o = \frac{D}{1-D} \cdot v_S(t), \quad (3)$$

where v_o is the output voltage also is the driving voltage on LED arrays.

2) Stage 2 [Q_1 off, see Fig. 7(b)]:

At the moment the Q_1 is turned off, the operation of the MSEBC in condition 1 enters into stage 2, in which all active switches are in off-state. The equivalent circuit is shown in Fig. 7(b). The inductors L_1 and L_2 start releasing energy but C_2 draws energy. The inductor L_1 dumps energy to capacitor C_1 and output by the path of C_1-D_5-C_2-v_s. The current following through L_1 decreases linearly under the assumption that v_{c1}, v_o, and v_s are constant within a switching period. There are two paths to release energy for L_2. One is the loop of D_5-C_2-L_2 to drive LEDs and the other is via the coupled-inductor L_3, battery, and D_{b2} to charge battery. If MSEBC functions as a power factor corrector incorporating BCM control, this stage will end at the moment i_{L1} drops to zero. If in PV mode, the termination of stage 2 depends on MPPT result.

In stage 2, the voltage across capacitor C_1 can be estimated from the loop, L_1-C_1-D_5-C_2-v_s and is expressed as

$$v_{C1}(t) = v_S(t) + L_1 \frac{di_{L1}}{dt} - v_{C2}(t). \quad (4)$$

According to the relationship between input and output of the MSEBC, the above equation can be rewritten as

$$v_{C1}(t) = \frac{1-2D}{1-D} v_S(t) + L_1 \frac{di_{L1}}{dt}. \quad (5)$$

From the energy-releasing path of the coupled inductor, the followings can be found.

$$v_{L3}(t) = V_{bat} - V_{f,Db2} \quad (6)$$

and

$$v_{L2}(t) = \frac{1}{n} \cdot k \cdot v_{L3}(t) = \frac{1}{n} \cdot k \cdot \left(V_{bat} - V_{f,Db2} \right), \quad (7)$$

where n is the turns ratio of the coupled inductor, V_{bat} represents the battery voltage, k denotes the coupling coefficient of the

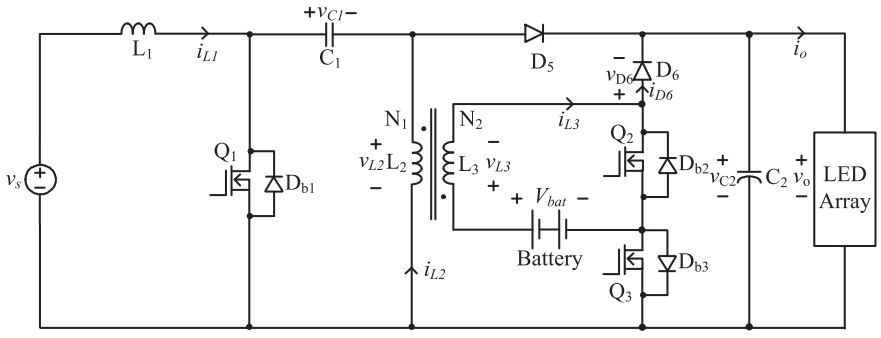

Fig. 6. The equivalent of the MSEBC working at utility mode or PV mode.

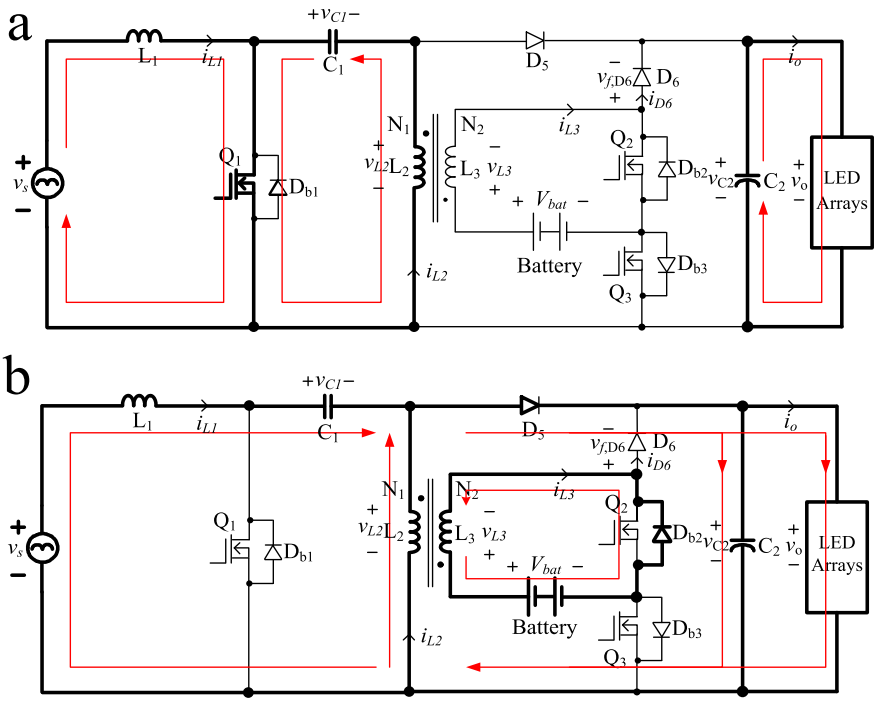

Fig. 7. The equivalents of the proposed converter operated in Condition 1. (a) Stage 1 and (b) Stage 2.

coupled inductor, and $V_{f,Db2}$ is the forward voltage of the parasitic diode of switch Q_2. The voltage v_{L2} can also be expressed as

$$v_{L2}(t) = v_{C2}(t) + V_{f,D5}, \tag{8}$$

in which $V_{f,D5}$ is the forward voltage of diode D_5. Therefore, the current of inductor L_3 is determined as follows:

$$i_{L3}(t) = i_{L3}(t_0) + \int_{t_0}^{t} \frac{V_{bat} - V_{f,Db2}}{L_3} dt = i_{L3}(t_0) + \int_{t_0}^{t} \frac{n \cdot V_{L2}(t')}{k \cdot L_3} dt'$$

$$= i_{L3}(t_0) + \int_{t_0}^{t} \frac{n \cdot v_{C2}(t') + V_{f,D5}}{k \cdot L_3} dt'$$

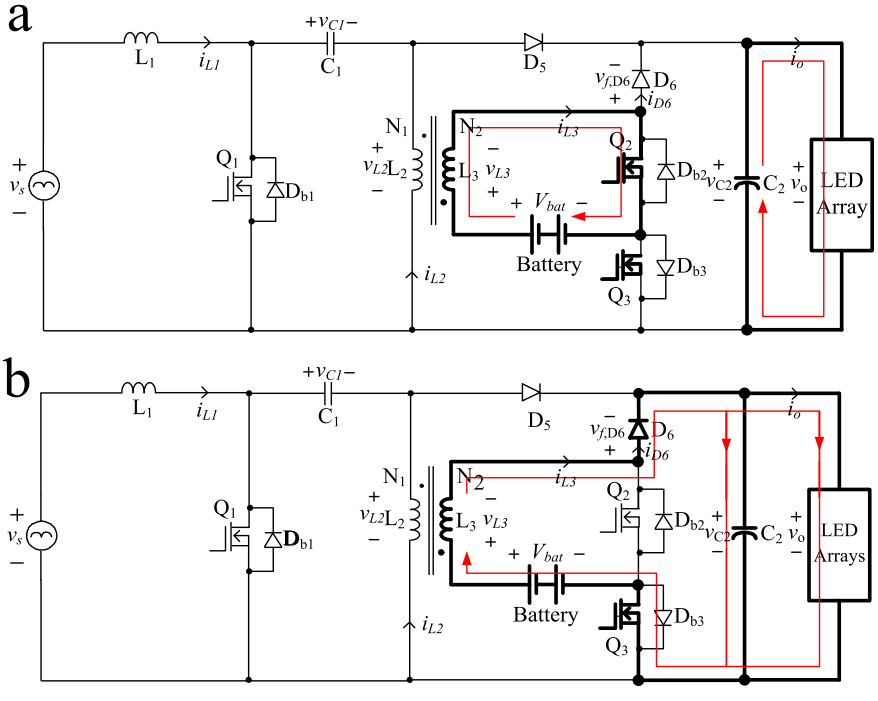

Fig. 8. The equivalents of the proposed converter operated in Condition 2. (a) Stage 1 and (b) Stage 2.

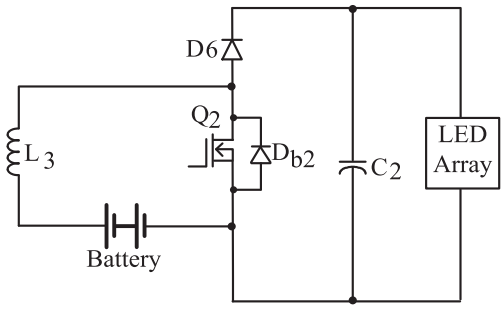

Fig. 9. The simplification of power stage of MSEBC operated in Condition 2.

3.2. Condition 2

During the interval of power failure and no irradiation, the MSEBC will operate in Condition 2, discharging battery energy to drive LED arrays for uninterruptible lighting feature. In Condition 2, the converter keeps Q_1 off. On the contrary, Q_3 is always closed so as to provide a battery discharge path. In addition, Q_2 is switched at high frequency. The MSEBC is controlled by constant frequency pattern and behaves as a boost converter to step up battery voltage.

According to the on or off of active switch Q_2, there are two stages to describe the working of the MSEBC.

1) Stage 1 [Q_2 on, see Fig. 8(a)]:

Since Q_2 is turned on, the battery is connected to the inductor L_3. The stored energy in L_3 increases and its current is linearly built. The voltage across the inductor L_3 can be described as

$$v_{L3}(t) = V_{bat} - V_{DS2,on}, \tag{10}$$

where $V_{DS2,on}$ denotes the on-state voltage of Q_2. Thus, the inductor current i_{L3} is estimated by

$$i_{L3}(t) = i_{L3}(t_0) + \int_{t_0}^{t} \frac{V_{bat} - V_{DS2,on}}{L_3} dt. \tag{11}$$

Owing to the output voltage is higher than battery voltage, in stage 1, even though Q_3 is kept in on-state, there is no current following through Q_3. During Condition 2, the Q_3 can be control at either always on to serve as a relay or high switching frequency complementary to Q_2. To reduce switching loss, the former control scheme is a prefer choice.

2) Stage 2 [Q_2 off, see Fig. 8(b)]:

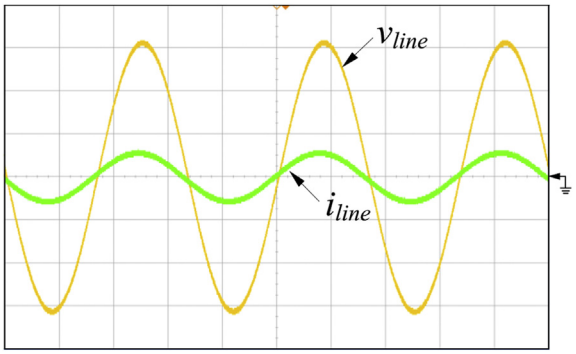

(v_{Line}: 50 V/div, i_{Line}: 2 A/div, time: 5 ms/div)

Fig. 10. Measured line voltage and line current.

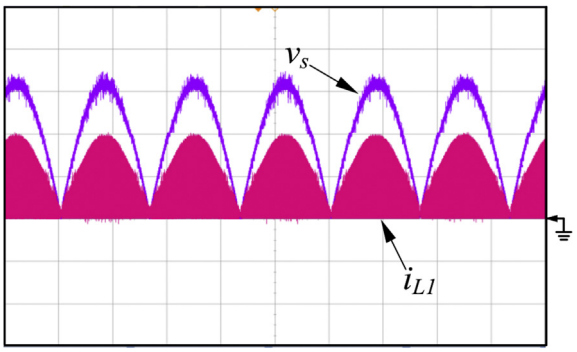

(v_s: 50V/div, i_{L1}: 1 A/div, time: 5 ms/div)

Fig. 11. Measured input inductor current.

While the switch Q_2 is turned off, the operation of the converter enters into stage 2. Since inductor current i_{L3} cannot change instantaneously, the diode D_6 becomes forward-biased to offer a path for inductor current i_{L3}. Kirchhoff's voltage law around the path containing inductor L_3, diode D_6, capacitor C_2, switch Q_3, and battery is

$$v_{L3}(t) = V_{DS3,on} + v_{C2} + V_{f,D6} - V_{bat}, \tag{12}$$

where $V_{DS3,on}$ is the turned-on voltage drop on Q_3 and $V_{f,D6}$ stands for the forward-biased voltage of D_6. Since v_{L3} is invariant, the rate of change of i_{L3} is a constant. That is, i_{L3} decreases linearly, which can be computed from

$$i_{L3}(t) = i_{L3}(t_1) + \int_{t_1}^{t} \frac{V_{DS3,on} + v_{C2} + V_{f,D6} - V_{bat}}{L_3} dt. \tag{13}$$

4. Design considerations

To simplify the circuit analysis, the following assumptions are made:

1) Steady-state conditions exist.
2) The voltages across C_1 and C_2 are considered as constants within one switching period.
3) Line frequency is far less than switching frequency.
4) All power components are ideal except the forward voltage of diode.

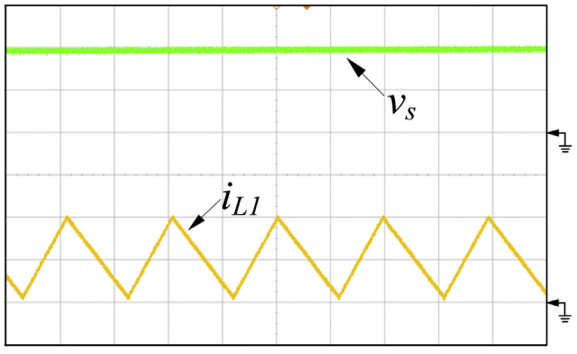

(v_s: 50 V/div, i_{L1}: 0.5 A/div, time: 10 μs/div)

Fig. 12. Zoomed-in waveform of input inductor current for the verification of BCM operation.

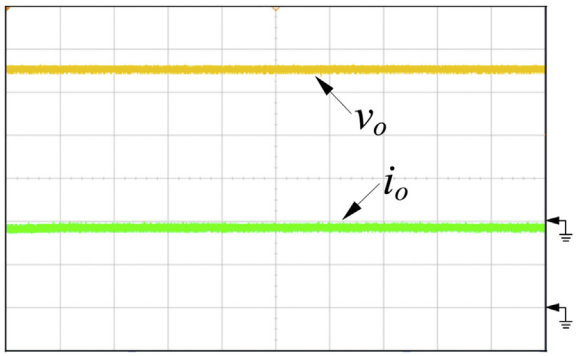

(v_o: 20 V/div, i_o: 200 mA/div, time: 20 μs/div)

Fig. 13. Measured LED driving voltage and current while MSEBC deals with line input.

4.1. Design for condition 1

At first, key parameters are listed as follows:

universal input voltage: $V_{s,min} \sim V_{s,max}$,
driving voltage for LEDs: V_o,
battery voltage: V_{bat},
load current: I_o,
battery current: I_{bat},
output power for LEDs: P_{LED},
battery charging power: P_{bat},
efficiency under Condition 1: η_1,
switching frequency of Q_1: $f_{sw1,min} \sim f_{sw1,max}$,
primary magnetizing inductance of coupled inductor: L_2,
secondary magnetizing inductance of coupled inductor: L_3,
input current ripple: Δi_{L1},
voltage ripple of capacitor C_1: Δv_{C1},
output voltage ripple: ΔV_o, and
duty ratio of Q_1: D_{Q1}.

The input inductance of an SEPIC converter can be calculated as follows:

$$L_{in} = \frac{\eta_1 \cdot D_{Q1} \cdot V_s^2 \cdot I_L}{\Delta i_{L1} \cdot f_{sw1} \cdot (P_{LED} + P_{bat})}, \tag{14}$$

where V_s and I_L denote the rms value of input voltage and the average of filtered input inductor current. Since load power equals the value of input power multiplied by efficiency, the above equation becomes

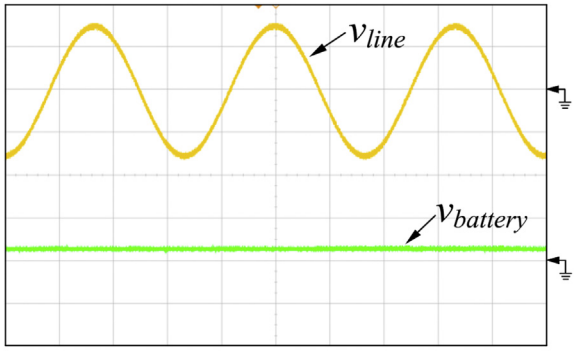

(v_{Line}: 100 V/div, v_{batter}: 100 V/div, time: 5 ms/div)

Fig. 14. Measured battery charging voltage and line voltage.

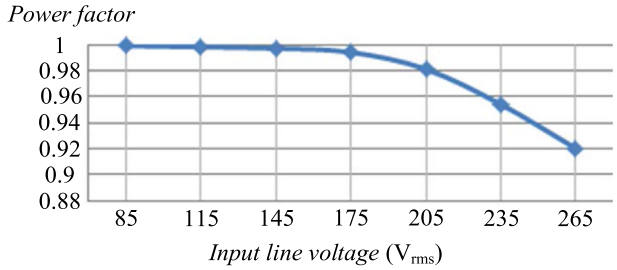

Fig. 15. Power factor measurement over universal line input.

$$L_{in} = \frac{D_{Q1} \cdot V_s}{\Delta i_{L1} \cdot f_{sw1}}. \tag{15}$$

While SEPIC performs power factor correction by BCM control, both duty ratio and switching frequency are varying. The minimum input inductance can be determined by

$$L_{in,min} = \frac{D_{Q1,max} \cdot V_{s,max}}{f_{sw1,min} \cdot (P_{LED} + P_{bat})}, \tag{16}$$

where $V_{s,max}$ and $f_{sw1,min}$ expresses the maximum rms value of input voltage and minimum switching frequency of Q_1, in turn. The choice of input inductance L_1 should be larger than $L_{in,min}$ and the inductance L_2 can be equal to L_1. That is,

$$L_1 = L_2 > L_{in,min}. \tag{17}$$

The relationship between input voltage and output voltage of SEPIC converter is found from the calculation of dividing duty ratio D by $(1-D)$. Thus, in equation (16), the computation of maximum duty ratio of Q_1 is

$$D_{Q1,max} = \frac{V_o + v_{f,D5}}{V_{s,min} + V_o + v_{f,D5}}. \tag{18}$$

The inductances of L_2 and L_3 can be expressed as

$$L_2 = \frac{L_{2,lk}}{1 - k^2}, \tag{19}$$

and

$$L_3 = \frac{L_{3,lk}}{1 - k^2}, \tag{20}$$

respectively, where $L_{2,lk}$ is the leakage inductance of the primary and $L_{3,lk}$ the leakage inductance of the secondary.

Because

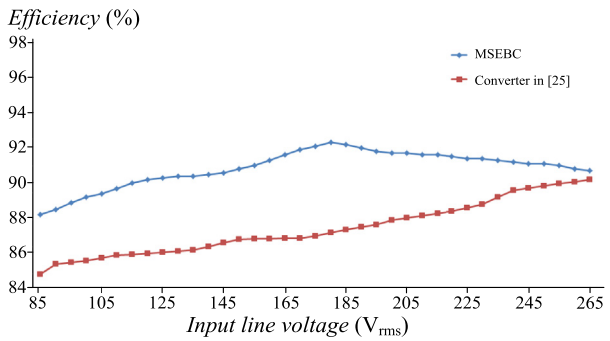

Fig. 16. Measured efficiency while the MSEBC performs power factor correcting.

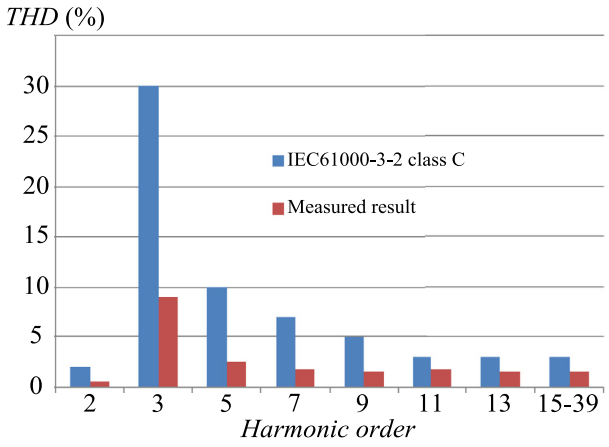

Fig. 17. Comparison of IEC 61000-3-2 class C standard with measured input current harmonics.

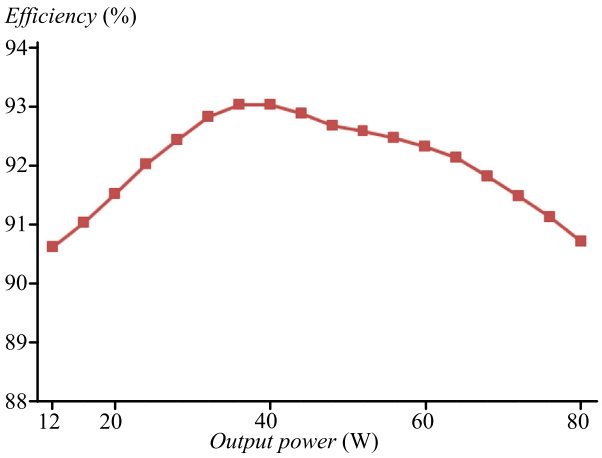

Fig. 19. Measured efficiency while the MSEBC processes PV power.

$$L_{3,\mathrm{lk}} = L_{2,\mathrm{lk}}(n)^2, \tag{21}$$

then the following holds

$$\frac{L_3}{L_2} = n^2. \tag{22}$$

When Q_1 is open, the voltage across the primary of coupled inductor is V_{LED} and the secondary voltage is V_{bat}. The ratio of V_{bat} to V_{LED} is

$$\frac{V_{\mathrm{bat}}}{V_{\mathrm{o}}} = n \cdot k, \tag{23}$$

where k is less than 1. Then, the following inequality yields

$$n^2 > \left(\frac{V_{\mathrm{bat}}}{V_{\mathrm{o}}}\right)^2. \tag{24}$$

Thus, we can selector the inductance of L_3 from

$$L_3 > L_2\left(\frac{V_{\mathrm{bat}}}{V_{\mathrm{o}}}\right)^2, \tag{25}$$

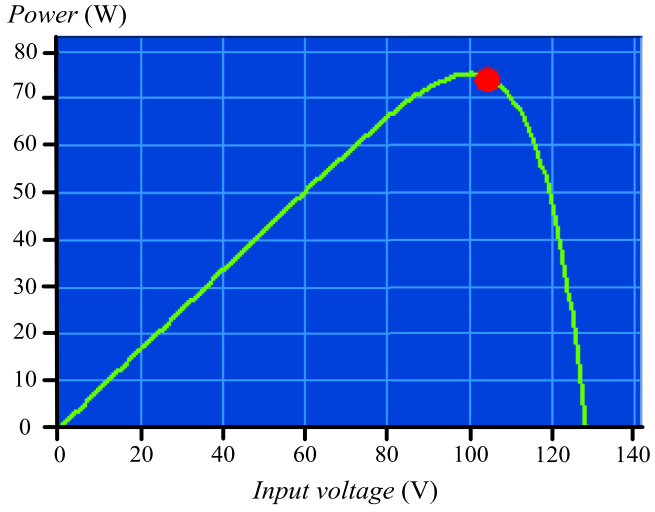

Fig. 18. Measured steady-state operation of the MSEBC with maximum power point tracking.

In the following, we will explore the determination for capacitances C_1 and C_2. With Coulomb's law, we can obtain a capacitance from the amount of charge that a capacitor can store and its terminal voltage, that is,

$$C = \frac{q(t)}{v_{\mathrm{C}}(t)}. \tag{26}$$

Accordingly, the capacitances C_1 and C_2 can be chosen from the relationships as follows:

$$C_1 > \frac{D_{\mathrm{Q1,max}} \cdot (I_{\mathrm{o}} + I_{\mathrm{bat}})}{\Delta v_{\mathrm{C1}} \cdot f_{\mathrm{sw1,min}}}, \tag{27}$$

and

$$C_2 > \frac{D_{\mathrm{Q1,max}} \cdot P_{\mathrm{LED}}}{\Delta V_{\mathrm{o}} \cdot f_{\mathrm{sw1,min}} \cdot V_{\mathrm{o}}}. \tag{28}$$

4.2. Design for condition 2

While MSEBC operates in Condition 2, the circuitry of its power stage can be simplified to the equivalent as shown in Fig. 9. From Fig. 9, it can be seen that the structure of MSEBC in Condition 2 is the same as that of a booster converter. Suppose that the efficiency of the MSEBC in Condition 2 is η_2 and the change of inductor current is Δi_{L3}. Then, the switching frequency of Q_2 is determined as

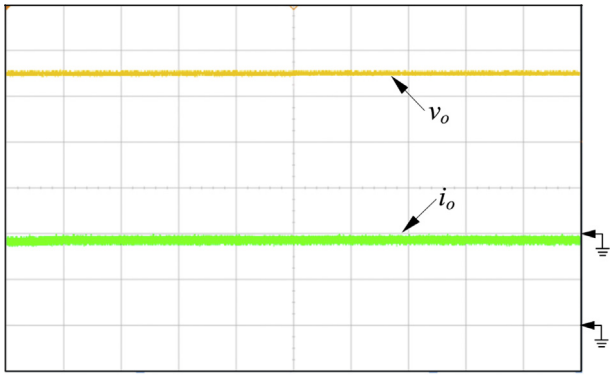

(v_o: 20 V/div, i_o: 200 mA/div, time: 20 μs/div)

Fig. 20. Measured LED driving voltage and current while MSEBC operates in discharging mode.

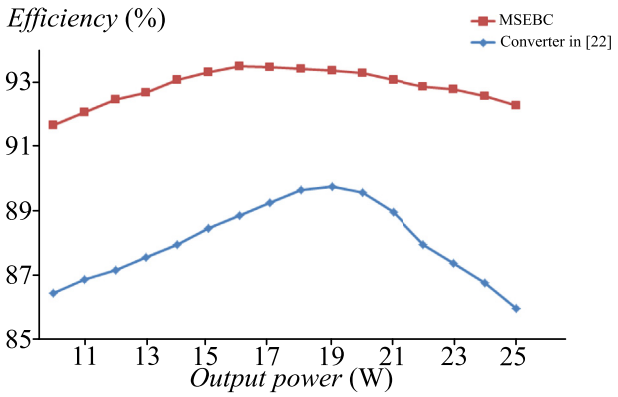

Fig. 21. Measured efficiency while the MSEBC operates in discharging mode.

$$f_{sw2} = \frac{D_{Q2} \cdot V_{bat}}{\Delta i_L \cdot L_3} \tag{29}$$

where D_{Q2} stands for the duty ratio of Q_2. From the following relations

$$P_{LED} = P_{bat} \cdot \eta_2, \tag{30}$$

and

$$P_{bat} = P_{LED} + P_{D6}, \tag{31}$$

We can obtain

$$V_{bat} \cdot I_{bat} = V_{bat} \cdot I_{bat} \cdot \eta_2 + I_{bat}(1 - D_{Q2}) \cdot v_{f,D6}. \tag{32}$$

In equation (31), P_{D6} is the power dissipation of diode D_6. Rearranging equation (32) gives

$$D_{Q2} = \frac{v_{f,D6} - V_{bat}(1 - \eta_2)}{v_{f,D6}}, \tag{33}$$

Based on the values of f_{sw2} and D_{Q2} obtained by equations (29) and (33), respectively, we also can find an appropriate magnitude for output capacitor C_2 as follows:

$$C_2' = \frac{D_{Q2,max} \cdot P_{LED}}{\Delta V_o \cdot f_{sw2} \cdot V_o}. \tag{34}$$

The larger capacitance computed from equations (28) and (34) will be adopted for C_2 in MSEBC.

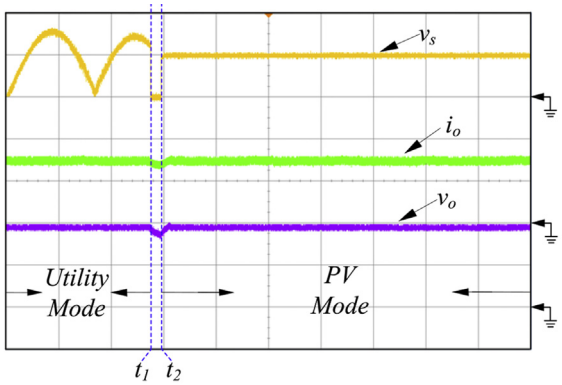

(v_s: 100 V/div, v_o: 50 V/div, i_o: 200 mA/div, time: 5 ms/div)

Fig. 22. The key waveforms of the transient response from utility mode to PV mode.

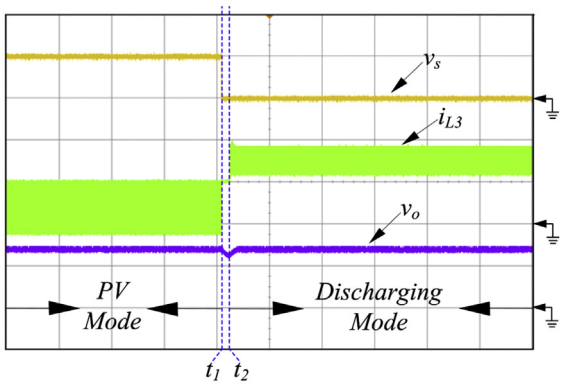

(v_s: 100V/div, v_o: 50 V/div, i_o: 200 mA/div, time: 5 ms/div)

Fig. 23. The key waveforms of the transient response from PV mode to charging mode.

5. Experimental results

A prototype of the MSEBC is built to demonstrate the theoretical analysis and to verify the feasibility. The controller of the prototype is implemented on a 16-bit disPIC-30F4011 chip, which fulfills all the controlling for Condition 1 and Condition 2. Specifications and circuit components are depicted as follows:

line input voltage: 85 ~ 265 V,
power rating: 80 W,
LED driving voltage: 72 V,
battery bank: 2 pieces in series (12 V/24 Ah for each piece),
LED: LUMILEDS 1 W/9 V/120 mA,
LED arrays: 3 strings, 8 pieces in series for each string,
Q_1: IRF840 (500 V/8 A),
Q_2: IRF640 (200 V/16 A),
Q_3: IRF640 (200 V/16 A),
$L_1 = 0.8$ mH, $L_2 = 0.8$ mH, $L_3 = 0.1$ mH,
$C_1 = 2.2$ μF, and $C_2 = 470$ μF.

In Condition 1, when the MSEBC is connected to mains to perform power factor correcting, Fig. 10 shows the experimental waveforms of line voltage and filtered line current. In addition, the corresponding input inductor current is shown in Fig. 11. From Fig. 10, it can be seen that the line current is sinusoidal and in phase with line voltage. Fig. 12 illustrates that the MSEBC indeed operates in BCM for PFC feature, which also verifies that the design of inductance L_1 of 0.8 mH is correct. Meanwhile, the LED driving voltage and current are presented as in Fig. 13 and battery charging voltage in Fig. 14. From Figs. 13 and 14, it can be observed that the MSEBC can provide constant outputs for both LED arrays and battery simultaneously even under sinusoidal input. In addition, the output voltage is around 72 V and battery charging voltage is about

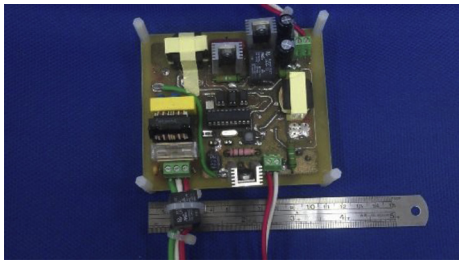

Fig. 24. The photograph of the proposed MSEBC.

27 V in Fig. 13, which indicates the validity of the designed inductances of L_2 and L_3. Over the line input range of 85 ~ 265 V, Figs. 15 and 16 show the measured power factor and efficiency, respectively. In Fig. 15, the highest power factor of the MSEBC is very close to unity and Fig. 16 reveals that the efficiency of the MSEBC in utility mode is over that of the converter in Ref. [25]. Fig. 17 demonstrates that the MSEBC can meet the requirement of standard IEC 61000-3-2 class C. While the MSEBC deals with PV power, perturb and observe method is adopted for maximum power point tracking. Fig. 18 shows the steady-state operation point with MPPT and measured efficiency is shown in Fig. 19. When operated in Condition 2, the MSEBC discharges battery energy to power LED arrays. Fig. 20 is the related driving voltage and current waveforms at full load and Fig. 21 shows the measured efficiency from light load to full load. The MSEBC is superior to the converter [22] in efficiency, which is also presented in Fig. 21. In Figs. 13 and 20, since the output voltage can be sustained at constant with very low ripples, it is obvious that the design values of C_1 and C_2 are appropriate. For dynamic characteristics illustration, Fig. 22 shows the transient response with respect to the operation-state change from utility mode to PV mode. In Fig. 22, the power failure is occurs at time t_1 and PV mode begins at time t_2. The mode-switched interval, from t_1 to t_2, is about 1 ms. After entering into PV mode, the MSEBC can reach steady state within 1 ms. The corresponding waveforms from PV mode to charging mode is shown in Fig. 23. It can be observed that the mode-switched interval, from t_1 to t_2, is within 1 ms and then, after t_2 the MSEBC has steady-state operation within in 1 ms. Fig. 24 is the photograph of the prototype, which indicates that the size of the MSEBC is 10 × 11.5 (W × L) cm^2.

6. Conclusion

The MSEBC is a totally novel power-supply system, which has dual input and dual outputs so as to deal with PV panel, utility, battery, and HB-LED in a single stage. The converter can perform power factor correcting while powered by utility and accomplishes MPPT while processing PV energy. A prototype is built and measured for demonstration. The practical results have verified its feasibility and validity. Key performances are summarized in the following. The corrected power factor can approach to unity and meets IEC commercial standard. In addition, MPPT efficiency is up to 99%. Regarding power conversion efficiency, while the MSEBC process utility power, it has a higher efficiency than conventional PFC by 4% at the input of 110 V_{rms}. While MSEBC deals with PV power, its efficiency is over than that of a conventional PV converter at least by 3.5%. In relating to dynamic characteristics, both transition times from utility mode to PV mode and from PV mode to discharging mode are less than 2 ms. That is, the MSEBC has a rapid dynamic response. To sum up, the proposed MSEBC is compact and cost-effective, possesses excellent performances and dynamic characteristics, and can accomplish multiple functions in a single stage.

References

[1] Huang T, Leu Y, Chang Y, Hou S. An energy harvester using self-powered feed forward converter charging approach. Energy 2013;55:769–77.
[2] Punitha K, Devaraj D, Sakthivel S. Artificial neural network based modified incremental conductance algorithm for maximum power point tracking in photovoltaic system under partial shading conditions. Energy 2013;62:330–40.
[3] Bouilouta A, Mellit A, Kalogirou SA. New MPPT method for stand-alone photovoltaic systems operating under partially shaded conditions. Energy 2013;55:1172–85.
[4] Tsai CT, Shen CL. High efficiency current-doubler rectifier with low output current ripple and high step-down voltage ratio. IEEJ Trans Electr Electron Eng (Industry Appl) 2013;8:182–9.
[5] Chen T, Ren T, Ou J. Fixed switching frequency applied in single-phase boost AC to DC converter. Energy Convers Manag 2009;50(10):2659–64.
[6] Dadouche F, Béthoux O, Kleider J. New silicon thin-film technology associated with original DC-DC converter: an economic alternative way to improve photovoltaic systems efficiencies. Energy 2011;36(3):1749–57.
[7] Genc N, Iskender I. An improved soft switched PWM interleaved boost AC-DC converter. Energy Convers Manag 2011;52(1):403–13.
[8] Wang H, Ren Z, Park J. Power electronic converters for microbial fuel cell energy extraction: effects of inductance, duty ratio, and switching frequency. J Power Sources 2012;220:89–94.
[9] Mirzaei A, Jusoh A, Zainal Salam Z. Design and implementation of high efficiency non-isolated bidirectional zero voltage transition pulse width modulated DC-DC converters. Energy 2012;47(1):358–69.
[10] Du Y, Lu DD. Battery-integrated boost converter utilizing distributed MPPT configuration for photovoltaic systems. Sol Energy 2011;85(9):1992–2002.
[11] Dargahi V, Sadigh AK, Pahlavani MRA, Shoulaie A. DC (direct current) voltage source reduction in stacked multicell converter based energy systems. Energy 2012;46(1):649–63.
[12] Tsai CT, Shen CL. A high step-down interleaved buck converter with active-clamp circuits for wind turbines. Energies 2012;5(12):5150–70.
[13] Tsai CT, Shen CL. Interleaved soft-switching buck converter with coupled inductors. WSEAS Trans Circuits Syst 2011;10(3):93–103.
[14] Moon SC, Koo GB, Moon GW. A new control method of interleaved single-stage flyback AC-DC converter for outdoor LED lighting systems. IEEE Trans Power Electron 2013;28:4051–62.
[15] Zhang J, Lu DD, Sun T. Flyback-based single-stage power-factor-correction scheme with time-multiplexing control. IEEE Trans Ind Electron 2010;57:1041–9.
[16] Fardoun AA, Ismail EH, Sabzali AJ, Al-Saffar MA. Bidirectional converter for high-efficiency fuel cell powertrain. J Power Sources 2014;249:470–82.
[17] Melo PF, Gules R, Romaneli EFR, Annunziato RC. A modified SEPIC converter for high power factor rectifier and universal-input voltage applications. IEEE Trans Power Electron 2010;25:310–21.
[18] Singh GK. Solar power generation by PV (photovoltaic) technology: a review. Energy 2013;53:1–13.
[19] Vasudeo V, Mohan A, Mohan K. Integrated battery controller for distributed energy system. Energy 2011;36(5):2392–8.
[20] Shin D, Kim Y, Wang Y, Chang N, Pedram M. Constant-current regulator-based battery-supercapacitor hybrid architecture for high-rate pulsed load applications. J Power Sources 2012;205:516–24.
[21] Kelly NA, Gibson TL. Solar photovoltaic charging of high voltage nickel metal hydride batteries using DC power conversion. J Power Sources 2011;196(23):10430–41.
[22] Tseng SY, Wang HY, Chen CC. PV power system using hybrid converter for LED indictor applications. Energy Convers Manag 2013;75:761–72.
[23] Huang BJ, Wu MS, Hsu PC, Chen JW, Chen KY. Development of high-performance solar LED lighting system. Energy Convers Manag 2010;51(8):1669–75.
[24] Shen CL, Chen KKA. Sepic-type single-stage electronic ballast for high line voltage applications. IEICE Trans Commun 2012:365–9. E95-B.
[25] Li YC, Chen CL. A novel single-stage high-power-factor AC-to-DC LED driving circuit with leakage inductance energy recycling. IEEE Trans Ind Electron 2012;59(2):793–802.